Macromolecules
ARTICLE

Macromolecules **2010**, *43*, 3479–3486 **3479**
DOI: 10.1021/ma902517v

Design of Soft and Strong Thermoplastic Elastomers Based on Nonlinear Block Copolymer Architectures Using Self-Consistent-Field Theory

Nathaniel A. Lynd,[†] Folusho T. Oyerokun,[†,⊥] Donal L. O'Donoghue,[†] Dale L. Handlin, Jr.,[‡,§] and Glenn H. Fredrickson*[,†]

[†]*Department of Chemical Engineering and the Materials Research Laboratory, University of California, Santa Barbara, California 93106, and* [‡]*Kraton Polymers LLC, 16400 Park Row, Houston, Texas 77084.* [§]*Formerly Kraton Polymers. Current address: PPG Industries, 940 Washburn Switch Road, Shelby, NC 28150.* [⊥]*Materials and Manufacturing Directorate, Air Force Research Laboratory, Wright-Patterson AFB, OH 45433-7132*

Received November 13, 2009; Revised Manuscript Received February 27, 2010

ABSTRACT: Thermoplastic elastomers (TPEs) that are soft at low extension yet strong at large extension are of great importance in a variety of technological applications. In ABA-triblock architectures, both the overall molecular weight and the composition of the glassy A-blocks correlate with TPE strength. The design space of current TPEs based on linear ABA triblock copolymers (e.g., polystyrene-*b*-polybutadiene-*b*-polystyrene) is restricted by the accessibility of the order−disorder transition temperature, limiting the molecular weight, and restricted by the maximum volume fraction for which glassy A-blocks will form discrete domains. Using self-consistent-field theory (SCFT), we designed *in silico* two new, nonlinear TPE architectures that significantly relax the composition restriction: radial $(ABA')_n$ and $A(BA')_n$ miktoarm star-block copolymers with chemically identical, but unequal, molecular weight A-blocks. Through a balance of end-block bidispersity, block extraction from the interface, and architectural asymmetry, these molecular architectures are able to stabilize phases with discrete A-rich domains at remarkably high overall A-monomer compositions (f_A). In some cases the maximum f_A achieved for phases with discrete A-rich domains surpasses twice that of conventional linear ABA TPEs.

Introduction

The most ubiquitous application of microphase-separated block copolymers is as thermoplastic elastomer (TPE) materials. Industrial applications of TPEs include rubber soles in footwear, asphalt modification, elastic film, soft molded parts, viscosity modification for oils and gels, and adhesives.[1] Conventional TPE designs generally consist of three or more blocks connected in a linear (regular or random) or grafted multiblock architecture with the requirements that terminal blocks form physical cross-links by segregating into discrete glassy or crystalline domains within a continuous matrix of the interior blocks that are rubbery at the service temperature.[2,3] Most of the commercially available poly(styrene)-*b*-poly(butadiene)-*b*-poly(styrene) (SBS) TPEs are based on linear ABA-triblock copolymer architectures consisting of two glassy polystyrene end blocks connected by an elastomeric polybutadiene middle block.[2,4] The mechanical strength of these materials is directly related to the overall molecular weight of the triblock copolymer and the total volume fraction of the glassy S blocks (f_S) that serve as physical cross-links. Access to the order−disorder transition temperature strictly limits the maximum melt-processable molecular weight of the neat materials. Additives such as oils and tackifying resins are commonly used to lower the ODT, but they typically lower strength by dilution. Hence, the development of TPEs based on SBS with low initial modulus but with high tensile strength and good processability necessitates increasing the glassy S-block composition while still maintaining discrete (spherical or cylindrical) S-domains, i.e., shifting phase boundaries to higher f_S.

The physical principles underlying the phase behavior of a linear ABA-triblock copolymer melt are similar to those of an AB diblock copolymer melt.[5,6] At sufficiently high segregation strength, defined by the product of the Flory−Huggins interaction parameter and the overall size of the polymer, χN, microphase separation between the incompatible A- and B-blocks will lead to formation of ordered morphologies (mesophases). The equilibrium mesophase is determined primarily by the relative composition of the blocks, as specified by volume fraction of each species $f_A = 1 - f_B$.[7] In melts of compositionally symmetric AB and ABA copolymers (i.e., $f_A \approx 0.5$), the copolymers segregate into a lamellar mesostructure with the junctions between the A- and B-blocks concentrated along the flat interfaces separating the microdomains. Microphase separation in compositionally asymmetric copolymers ($f_A \neq 0.5$) results in formation of mesophases with curved AB-interfaces in which the longer blocks reside on the convex side of the curved interface because it affords them more configurational entropy.[8] The shorter blocks pack within the interior of the curved interface to form discrete domains embedded in the matrix of the larger block.[9,10] In general, the range in composition over which discrete A-domains are obtainable is relatively small, typically $0.1 \leq f_A \leq 0.3$. This imposes limitations on the modulus/tensile strength balance obtainable from processable materials based on linear ABA copolymer architectures.

Recent studies have shown that the order−order transitions (OOTs) in linear AB-diblock copolymers can be modified via introduction of discrete or continuous polydispersity in one of the blocks.[11−17] Matsen has done extensive self-consistent-field theory

*To whom correspondence should be addressed. E-mail: ghf@mrl.ucsb.edu.

Published on Web 03/11/2010

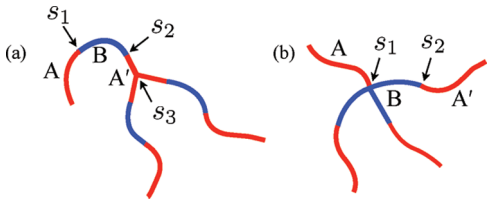

Figure 1. Schematic diagram of TPE architectures: (a) $(ABA')_n$ radial star-block copolymer shown with $n = 3$. (b) $A(BA')_n$ miktoarm star-block copolymer with $n = 3$. Both structures are characterized by the total composition of A-block and A′-block (f_A) and the bidispersity between the A- and A′-blocks, $\tau \equiv N_A/(N_A + N_{A'})$. Block junctions, s_i, are labeled for each structure.

(SCFT) calculations on the role of asymmetry in molecular weight of the terminal A-blocks on the equilibrium phase behavior of ABA′-triblock copolymers.[18] Here and throughout, A′ denotes a block chemically identical to A, but with a distinct molecular weight. Matsen found that at modest bidispersity of the A end blocks, deflections in phase boundaries toward higher f_A occur. These deflections are driven primarily by the reduction in the stretching energy of the A-rich domain due to the bidisperse A-blocks which favors curving the interface toward the A-rich domain. However, for sufficiently bidisperse end blocks, Matsen predicted that the shorter A-block will be extracted from the interface into the B-rich domain. Extraction of the short A-blocks into the majority B-rich domain occurs because the reduction in unfavorable segment−segment contacts can no longer be balanced by the entropic cost of stretching the short A-block from the interface. The segregation of the shorter A-block into the interior of the B-rich domain is accompanied by a decrease in the stretching energy of the B-rich domain. Thus, extraction leads to a shift in phase boundaries back toward lower f_A (higher f_B). The maximum shifts in the phase boundaries were found to coincide with the onset of the pullout of the short A-block. The extraction of A-blocks limits the application of asymmetric ABA′ in TPEs because of the commensurate reduction in the fraction of B-blocks that bridge between the discrete A-rich microdomains that is known to correlate directly with elastomer strength.[19]

In this report, we investigate TPE designs based on two block copolymer architectures that utilize bidispersity of the terminal A-blocks (A and A′) in nonlinear molecular architectures to shift phase boundaries toward higher volume fraction of the A-blocks (f_A). The architectures studied are a radial $(ABA')_n$ and a miktoarm $A(BA')_n$ star-block copolymer (see Figure 1). The motivation behind the $(ABA')_n$ radial block design is to suppress extraction of the short A′-blocks into the B-rich domain by linking n ABA′-triblock copolymers at the A′ termini to form a radial molecular architecture. In such an architecture, even if extraction of the A′-blocks were to occur, the longer outer A-blocks would provide an anchoring effect to maintain strength. The $A(BA')_n$ miktoarm star-block design is inspired by studies done on $(A)_m(B)_n$ miktoarm star-block copolymers where significant deflections in phase boundaries toward higher f_A have been predicted and observed when $n > m$.[20−23] Because of the steric hindrance about the junction between the A- and B-blocks in an $A(B)_n$ miktoarm copolymer, a prohibitive degree of chain stretching is required to pack the n (>1) B-blocks on flat interfaces. This steric hindrance strongly favors mesophases where the n B-blocks are allowed to relax on the convex side of the AB-interface. While such $A(B)_n$ miktoarm polymers show discrete A domains at higher f_A than conventional AB-diblocks or ABA-triblocks, they are not suitable as elastomers because they do not have anchoring glassy A-blocks. In contrast, our $A(BA')_n$ miktoarm star-block design has anchoring A and A′ end blocks, so it should perform as a true TPE. Moreover, for suitable ratios of A- and A′-block molecular weight, we expect

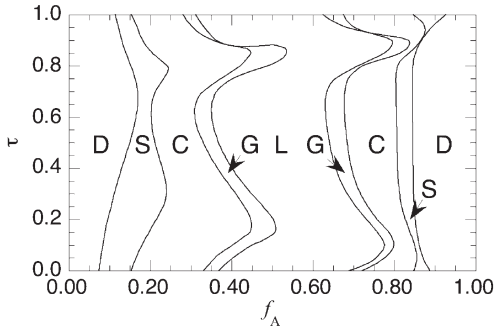

Figure 2. Phase diagram for $(ABA')_3$ at $\chi N_{ABA'} = 40$ as a function of τ and f_A calculated using SCFT. Large deflections in phase boundaries toward higher f_A occur at $\tau \approx 0.8-0.9$ and $\tau \approx 0.1-0.2$. The large deflections in phase boundaries result from a competition between the bidispersity between the A- and A′-blocks and pullout of the shorter A- or A′-block in asymmetric ($\tau \neq 0.5$) radial copolymers.

that the block bidispersity effect studied by Matsen should reinforce the *miktoarm effect* just described to produce stabilization of discrete A-domains to unprecedented values of f_A. As described below, detailed SCFT calculations support this conjecture.

Results and Discussion

The first architecture considered consists of $n \geq 3$ linear ABA′-triblock copolymers joined together at their A′ termini (Figure 1a) to form an $(ABA')_n$ radial copolymer structure where the size of the A′-block is distinct from the A-block. Each ABA′-triblock arm of the radial copolymer contains $N_{ABA'} \equiv N_A + N_B + N_{A'}$ segments, so that the total number of segments is $N = nN_{ABA'}$. The volume fraction of A segments in the $(ABA')_n$ radial copolymer architecture is $f_A = n(N_A + N_{A'})/N = (N_A + N_{A'})/N_{ABA'}$. Note that for the special cases of $n = 1$ and $n = 2$ the radial copolymer design reduces to linear ABA′-triblock and ABA′A′BA hexablock copolymers, respectively.

The second architecture studied consists of a single A-homopolymer block bound at one of its ends to the B-block ends of n BA′ diblock copolymers (Figure 1b) to form an $(n + 1)$-arm miktoarm copolymer structure, $A(BA')_n$. Each BA′ arm of the miktoarm copolymer has $N_{BA'} \equiv N_B + N_{A'}$ segments so that the total number of segments is $N = N_A + nN_{BA'}$. The total volume fraction of A segments in the miktoarm star-block architecture is $f_A = (N_A + nN_{A'})/N$. Following the notation of Mayes and Olvera de la Cruz, the bidispersity of the two distinct A-blocks in each copolymer chain is described by $\tau \equiv N_A/(N_A + N_{A'})$, where $0 \leq \tau \leq 1$.[24]

Self-consistent-field theory (SCFT) has been used successfully to predict phase behavior of linear,[25] graft, and star-block copolymers.[23] Detailed descriptions of SCFT and its numerical implementation are available elsewhere.[6,10,25−30] In the present study, we primarily used the spectral method of Matsen and Schick[30] and also the pseudospectral method of Ceniceros and Fredrickson[29] to investigate the phase behavior of the $(ABA')_n$ radial and $A(BA')_n$ miktoarm copolymer architectures as a function of composition f_A, bidispersity τ, arm number n, and segregation strength χN. Basis functions for the spectral method were generated using the method of Tyler and Morse.[32] The free energies were determined in unit cell calculations after minimization with respect to the domain spacing D^* of the periodic ordered structures. To construct phase diagrams, we compared the free energies of the disordered state (DIS), body-centered-cubic spheres (S), hexagonally packed cylinders (C), gyroid (G), and lamellar (L) morphologies to an accuracy of at least 10^{-4} in free energy per chain (kT units) at the highest segregation strength. We have not explored the stability of nonclassical

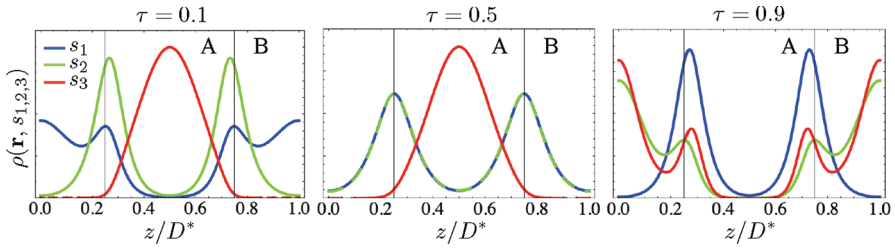

Figure 3. Junction distributions within a single period of the lamellar structure at $\chi N_{ABA'} = 40$, $f_A = 0.5$, and $n = 3$ for the $(ABA')_3$ radial architecture. The junctions are labeled according to Figure 1a. The interfaces between the A- and B-rich domains are indicated with vertical lines. At $\tau = 0.1$ the s_1 junctions between the A- and B-blocks are primarily pulled free of the interface within the B-rich domain. The s_2 junctions between the B- and A′-blocks are primarily located at the AB-interface, and the s_3 junction at the linkage between the three A′-blocks is located within the center of the A-rich domain. At $\tau = 0.5$ both the s_1 and s_2 junctions are equivalently located at the AB-interface. The s_3 junction is located at the center of the A-rich domain. At $\tau = 0.9$, where the A-block is much larger than the A′-block, the s_1 junction is firmly located at the AB-interface, and the s_2 and s_3 junctions have become dislodged from the AB-interface and are embedded within the B-rich domain. This is consistent with the entire A′-bridge pulling free of the AB-interface.

morphologies such as the perforated lamella and A15 packing of the spherical domains.[6,18,23,33]

Phase Behavior of the $(ABA')_n$ Radial Copolymer. Figure 2 shows the phase diagram for the $(ABA')_3$ melt system at $\chi N_{ABA'} = 40$ (i.e., χN per ABA′ arm of the copolymer) calculated by SCFT as a function of f_A and τ. As τ deviates from 0.5, the phase boundaries shift toward higher f_A. The origin of the shifts in the phase boundaries at intermediate τ (0.20−0.75) is similar to the reasons behind the shifts in phase boundaries in the linear ABA′.[18] As τ deviates from 0.5 and bidispersity in the terminal A- and A′-blocks increases, the A-rich domain gains conformational entropy due to the mixing of chains of different size; this stabilizes structures where the A- and A′-blocks are on the concave side of the interfaces.[34] The softening of the A-rich domain then shifts phase boundaries toward higher f_A. As bidispersity increases further ($\tau > 0.75$, $\tau < 0.20$), extraction of the shorter block (A at $\tau < 0.20$, A′ at $\tau > 0.75$) allows the B-blocks to relax as the short A- or A′-segments segregate to the extremities of the B-rich domain. This release in stretching of the B-rich domain relative to the A-rich domain shifts phase boundaries back toward lower f_A. The maximum shift in phase boundaries to higher f_A, the most desirable set of conditions for TPEs with the $(ABA')_3$ architecture, occurs near $\tau = 0.85$ where the effects of A-block bidispersity balances extraction from the interface. From the application standpoint, it is fortunate that the maximum shift in f_A occurs for $\tau > 0.5$, which puts the longer A-blocks on the periphery of the molecule and should lead to enhancement in strength relative to molecules with $\tau < 0.5$. For $\tau \approx 0.9$ where the A′-blocks dislodge from the interface, G became completely unstable and gave way to a direct C to L transition. The limitations of the spectral method preclude us from knowing *a priori* if some other phase becomes stable in these regions of the phase diagram unless we calculate the free energies of all candidate structures, a computationally intensive and laborious task. This region of the phase diagram will be the subject of more comprehensive investigations in the future.

The densities of the s_1, s_2, and s_3 junctions within a lamellar unit cell are shown in Figure 3 at three values of τ with $n = 3$, $f_A = 0.5$, and $\chi N_{ABA'} = 40$. One period of the lamellar structure is shown with the interfaces between the A- and B-rich domains indicted by vertical lines. At $\tau = 0.1$, the A-blocks are much smaller than the A′-blocks. As a result, the junction between the A- and B-block (s_1) is located both at the interface and partially extracted to the center of the B-rich domain at $z/D^* = 0$ and 1. The junction between the B-blocks and longer A′-blocks (s_2) is firmly anchored at the AB-interface, and the junction between the A′-blocks (s_3) is

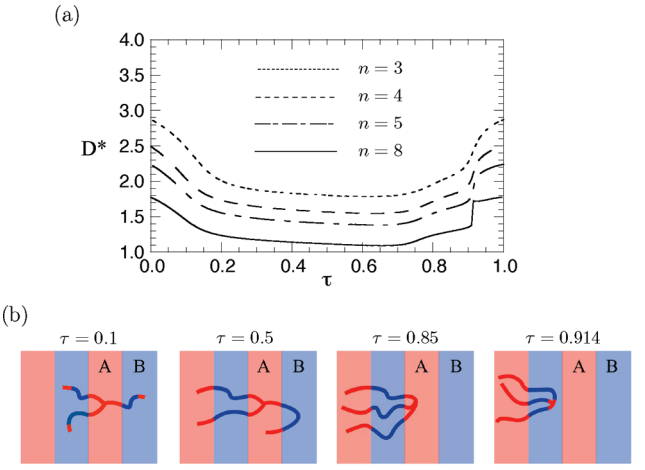

Figure 4. Effect of n on the lamellar domain spacing for the $(ABA')_3$ radial triblock copolymer; the lamellar domain spacing D^* vs bidispersity τ at $\chi N_{ABA'} = 40$ and $f_A = 0.6$: $n = 3$ (dotted line), $n = 4$ (dashed line), $n = 5$ (dot-dashed line), $n = 8$ (solid line). D^* increases precipitously at $\tau < 0.2$ due to extraction of the short A-block from the interface and at $\tau > 0.7$ due to A′-bridge migration to the interface followed by A′-bridge extraction from the AB-interface into the B-domain at $\tau = 0.91$. D^* is given in units of the unperturbed radius of gyration.

predominantly located in the center of the A-rich domain. At $\tau = 0.5$ the A- and A′-blocks have the same size. The s_1 and s_2 junctions are partitioned identically at the AB-interface. At the other extreme of $\tau = 0.9$ the A′-block is much smaller than the A-block. The s_1 junction is predominantly located at the AB-interface whereas the majority of both the s_2 and s_3 junctions are located in the center of the B-rich domain. This is consistent with the nearly complete extraction of the A′-bridge into the B-rich domain.

Matsen noted that the extraction of short A-blocks into the B-rich domain at low τ in linear ABA′-triblock copolymers was accompanied by a precipitous growth in the domain spacing of the equilibrium mesophase.[18] The short, extracted A-blocks locate primarily in the extremities of the B-rich domain where B-blocks would otherwise be required to unfavorably stretch, thus increasing the conformational entropy of the mesophase and stabilizing a larger domain spacing. Block extraction may thus be probed by calculating the equilibrium domain spacing as a function of the number of arms n and τ.

Figure 4 shows the lamellar domain spacing (D^*) as a function of τ for the radial $(ABA')_n$ architecture at $f_A = 0.5$ and $\chi N_{ABA'} = 40$ for $n = 3$, 4, 5, and 8. For $\tau < 0.2$, the

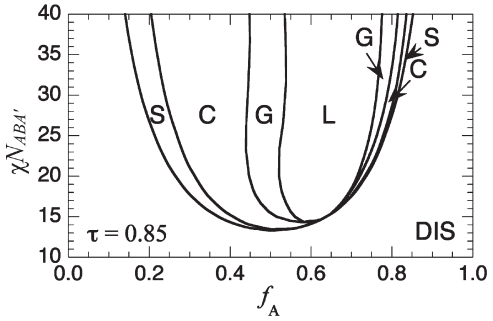

Figure 5. Phase diagram for $(ABA')_3$ at fixed $\tau = 0.85$ corresponding approximately to the maximum deflection in the C → G → L phase boundaries in Figure 2.

increase in D^* is approximately unaffected by variation in n. This implies that the extraction of the A-block from the AB-interface is independent of the number of arms. The increase in D^* for $\tau > 0.7$ occurs in two stages and is shown schematically in Figure 4b. In the first stage, the increase in D^* is driven by the bridge formed by the short, linked A′-blocks migrating from spanning the length of A-rich domain to localizing at an AB-interface. This migration is required since the A′-bridge may no longer stretch across the entire A-rich domain as its size decreases relative to the thickness of the A-rich domain. The second and more abrupt change in D^*, which occurs at $\tau \approx 0.91$, is due to the extraction of the entire A′-bridge from the AB-interface into the B-rich domain. Although the extraction of the A′-bridge becomes more discontinuous as n is increased, the location of extraction did not change appreciably with n. The value of τ at the onset of A- or A′-block extraction corresponds to the maximum deflection in the phase boundaries toward higher f_A. Preliminary calculations of the metastable C to L transitions (see Supporting Information Figure 1) demonstrated that the bidispersity τ at the maximum shift in the phase boundary toward higher f_A did not deviate from $\tau = 0.85$ with $n \geq 3$. The volume fraction f_A at the C to L transition changed slightly from approximately 0.495 to 0.507 as n was increased from 3 to 5 at $\tau = 0.85$. The shift in f_A at the C to L transitions with variations in n at $\tau \approx 0.15$ was of a similar magnitude.

We note that the phase diagram, extraction boundaries, and domain spacing variations depend in quantitative detail on the choice of segregation strength, $\chi N_{ABA'} = 40$. While we expect qualitatively similar trends at higher segregation strengths, the laborious task of comprehensively mapping these out was not part of this investigation. The value of $\chi N_{ABA'} = 40$ was selected as representative of a moderate segregation strength for which a system could be designed to disorder at elevated temperature and thereby facilitate melt processing. This order−disorder envelope and the associated phase boundaries at lower values of $\chi N_{ABA'}$ are the next subject of discussion.

An understanding of the phase behavior at lower $\chi N_{ABA'}$ is necessary for proper molecular design and high-temperature processing of TPEs based on $(ABA')_n$ copolymer architectures. Figure 5 shows the phase diagram of the $(ABA')_3$ starblock architecture plotted as a function of $\chi N_{ABA'}$ and f_A at approximately the optimum bidispersity ratio for affecting rightward shifts in the phase boundaries, $\tau = 0.85$. At intermediate values of $\chi N_{ABA'}$ ($26 < \chi N_{ABA'} < 35$), the gyroid window shifts slightly toward larger f_A. Investigation of the lamellar structure with $f_A = 0.6$ as $\chi N_{ABA'}$ is changed sheds some light on the shift in phase boundaries. D^* vs $\chi N_{ABA'}$ at $\tau = 0.85$ and $f_A = 0.6$ is shown in Figure 6. At $\chi N_{ABA'} = 20$,

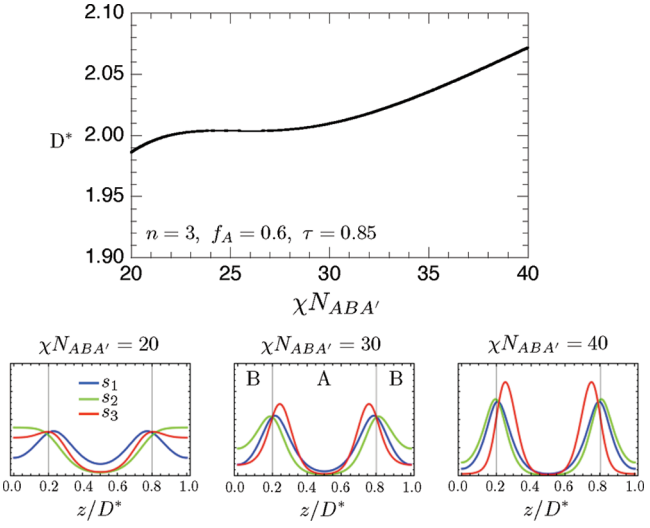

Figure 6. Lamellar domain spacing D^* vs $\chi N_{ABA'}$ with $n = 3$, $f_A = 0.6$, and $\tau = 0.85$. Junction density distributions at three segregation strengths are shown below ($\chi N_{ABA'} = 20$, 30, and 40) with the location of the AB-interfaces indicated by vertical lines. At $\chi N_{ABA'} = 20$, the mesophase is weakly segregated and the A′-bridge is predominantly located within the B-rich domain. By $\chi N_{ABA'} = 30$, the A′-bridge has partially migrated to the interface but does not extend across the entire A-rich domain. This rearrangement suppresses the growth of domain spacing with $\chi N_{ABA'}$. By $\chi N_{ABA'} = 40$ the A′-bridge is firmly located near the AB-interface. Domain spacings (D^*) are given in units of the unperturbed radius of gyration.

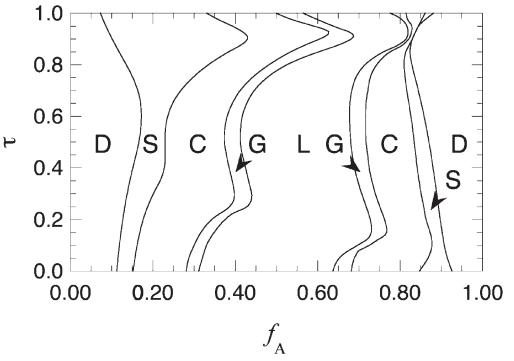

Figure 7. Phase diagram for $A(BA')_3$ miktoarm starblock architecture at $\chi N_{ABA'} = 40$, as a function τ and f_A. The phase boundaries are shifted to higher f_A as τ diverges from 0.5. The maxima in the deflections in phase boundaries result from a competition between the bidispersity between the A- and A′-blocks and pullout of the shorter A- or A′-block. The shift in phase boundaries at $\tau \approx 0.9$ is disproportionately large due to suppression of A′-block extraction from the AB-interface far from $\tau = 0.5$ and the inherent architectural asymmetry of the miktoarm copolymer.

the mesostructure is weakly segregated and the A′-bridge is located predominantly within the B-rich domain. As $\chi N_{ABA'}$ is increased, D^* slightly increases and eventually reaches a plateau near $\chi N_{ABA'} = 24$ due to the rearrangement of the A′-bridge from the B-rich domain to the AB-interface. The rearrangement of the A′-bridge corresponds to the anomalous shift in the gyroid window back toward lower f_A as the A-rich domain is relaxed relative to the B-rich domain. By $\chi N_{ABA'} = 27$, the A′-bridge rearrangement is sufficient to allow D^* to resume increasing as $\chi N_{ABA'}$ is increased. In Figure 2 of the Supporting Information, we show the dependence of D^* on τ at $\chi N_{ABA'} = 20$, 30, and 40 for $n = 3$, 4, and 5. Only near the maximum deflection in the phase boundaries does D^* not exhibit a monotonic increase with $\chi N_{ABA'}$.

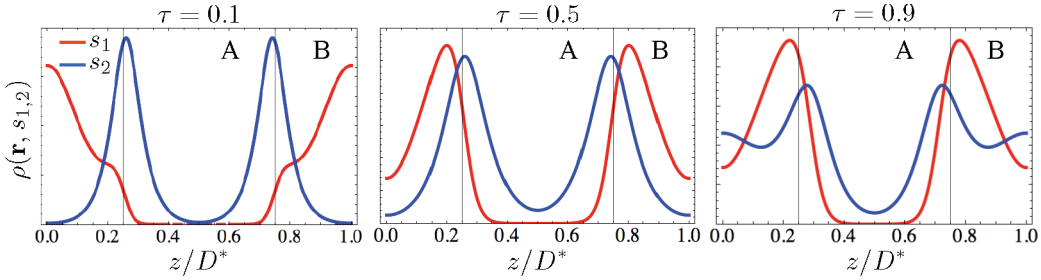

Figure 8. Junction distributions within a single period of the lamellar structure at $\chi N_{ABA'} = 40$, $f_A = 0.5$, and $n = 3$ for the A(BA′)$_n$ miktoarm architecture. The junctions are labeled according to Figure 1b. The interfaces between the A- and B-rich domains are indicated with vertical lines. At $\tau = 0.1$, the A-block is much smaller than the A′-blocks, and the s_1 junction is pulled free of the AB-interface into the B-rich domain. A-block extraction is driven by the release of steric hindrance at the AB-interface due to the architectural asymmetry in the miktoarm system. At $\tau = 0.5$ both the s_1 and s_2 junctions are located near the interface. The s_2 junction is driven by the steric hindrance at the interface to be concentrated slightly in the B-rich domain in agreement with Grason and Kamien.[23] At $\tau = 0.9$, where the A-blocks are much larger than the A′-blocks, the s_2 junctions are becoming dislodged from the AB-interface.

Although increasing n did not bring about a further suppression of A′-block extraction toward higher τ or produce a larger shift in phase boundaries toward larger f_A, the radial ($n \geq 3$) copolymer system has the potential to outperform the linear ABA′-copolymer-based TPEs. Extraction of A′-blocks from the AB-interface is suppressed at higher τ where the A′-block is smaller than the A-block, and morphologies with discrete A-rich domains are stable to higher f_A than the linear ABA′-triblock copolymer system. Moreover, extraction of the A′-blocks would not necessarily lead to a catastrophic loss of strength in (ABA′)$_n$ architectures with $n \geq 2$, whereas this would most certainly be the case for an ABA′-triblock. Finally, we note that in the case of styrenic elastomers the anionic polymerization of a radial (SBS′)$_n$ architecture can be accomplished by terminating the corresponding polymerization of a linear SBS′ copolymer with an n-functional coupling agent such as a chlorosilane in stoichiometric deficiency.[35]

Phase Behavior of Miktoarm A(BA′)$_n$ Copolymer. The phase diagram for the A(BA′)$_3$ miktoarm architecture at $\chi N_{ABA'} = 40$ as a function τ and f_A is shown in Figure 7. The topology of the phase diagram is similar to that for the (ABA′)$_3$ radial architecture; there are two prominent deflections in phase boundaries toward larger f_A at high and low τ. However, in the present miktoarm case the shift in phase boundaries at $\tau = 0.9$ is disproportionately larger than the shift at $\tau \leq 0.5$. To investigate the underlying causes of the topology of the phase diagram, the junction distributions within a lamellar unit cell are shown in Figure 8 at $f_A = 0.5$ and $\tau = 0.1$, 0.5, and 0.9. As τ is varied at fixed composition f_A and $\chi N_{ABA'}$, three regimes of behavior are observed. At $\tau \approx 0.1$, the s_1 junction between the A- and B-blocks is not constrained to the interface and is concentrated in the center of the B-rich domain. The extraction of the A-block relieves the interfacial crowding on the AB-interface of the miktoarm architecture. Thus, a large amount of conformational entropy is gained when the A-block is extracted from the interface. The s_2 junction between the B- and A′-blocks is firmly located at the interface. At an intermediate $\tau \approx 0.5$, both the s_1 and s_2 junctions are located at the interface. The s_1 junction is not concentrated exactly on the AB-interface but is located slightly behind the AB-interface into the B-rich domain. This is the result of the strong steric hindrance at the crowded s_1 junction. Concentrating the s_1 junction slightly behind the AB-interface does incur unfavorable AB contacts but relieves some of the unfavorable stretching that would be required to place the sterically hindered s_1 junction directly on the interface. Grason and Kamien noted this effect in their study of conventional

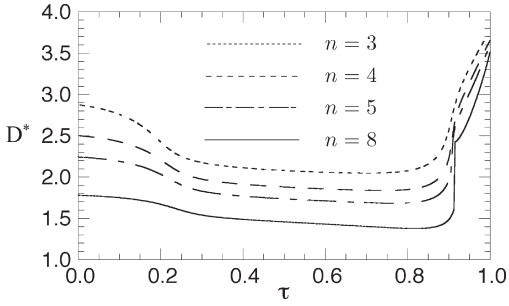

Figure 9. Effect of n on the lamellar domain spacing for the A(BA′)$_3$ miktoarm star triblock copolymer; the lamellar domain spacing D^* vs bidispersity τ at $\chi N_{ABA'} = 40$ and $f_A = 0.5$: $n = 3$ (dotted line), $n = 4$ (dashed line), $n = 5$ (dot-dashed line), $n = 8$ (solid line). D^* increases at $\tau < 0.25$ due to extraction of the A-block from the interface and at $\tau > 0.85$ due to A′-block extraction into the B-rich domain at $\tau = 0.91$. At both low ($\tau < 0.25$) and high τ ($\tau > 0.85$), increasing n shifts A-block extraction toward higher τ. Domain spacings (D^*) are given in units of the unperturbed radius of gyration.

(A)$_m$(B)$_n$ miktoarm copolymers as well.[23] At $\tau \approx 0.9$, the s_2 junction begins to dislodge from the AB-interface. However, the smaller A′-blocks require a larger bidispersity to dislodge from the interface than the A-blocks; i.e., they require a greater difference from $\tau = 0.5$ to make their extraction from the AB-interface energetically favorable. This is because there is no interfacial crowding driving their extraction. As τ increases further, the s_2 junctions pull free of the interface and partition within the center of the B-rich domain. This partitioning relaxes the B-rich domain relative to the A-rich domain and begins shifting phase boundaries back toward lower f_A. Thus, both the maximum shifts in phase boundaries toward higher f_A that occur near $\tau \approx 0.9$ and $\tau \leq 0.5$ represent a balance between the A- and A′-block bidispersity relaxing the A-rich domain shifting phase boundaries toward larger f_A, and the A- or A′-block extraction that relaxes the B-rich domain shifting phase boundaries back toward lower f_A.

The technologically relevant S to C and C to G phase boundaries at $f_A = 0.43$ and 0.60, respectively, both at $\tau = 0.9$, correspond to roughly *twice* the maximum A-monomer loadings (f_A) possible in the linear ABA′-triblock and the (ABA′)$_3$ copolymer at the same segregation strength.[18] Thus, the A(BA′)$_n$ miktoarm architecture is a very promising polymer structure to engineer TPE materials that are strong due to the high loading of A-monomer, soft due to the discreteness of the A-rich domains, and processable due to an accessible T_{ODT}.

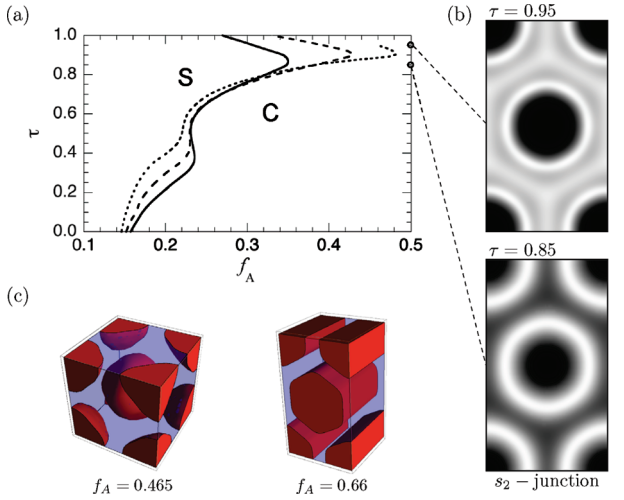

Figure 10. (a) The S to C phase boundary for $n = 2$ (solid line), 3 (dashed line), and 5 (dotted line). Increasing n causes the S to C phase boundary in the upper half of the phase diagram ($\tau > 0.5$) to shift toward higher f_A. S is stable at very high $f_A = 0.48$ at $\tau = 0.9$ and $n = 5$. (b) s_2 junction density between the B- and A′-blocks within a C unit cell at $\tau = 0.85$ and $\tau = 0.95$. The furthest deflection in phase boundaries at $\tau \approx 0.9$ corresponds to the onset of extraction of the s_2 junction. (c) Real-space renderings of unit cells at $\tau = 0.9$ for S ($f_A = 0.465$) and C ($f_A = 0.66$) with $n = 5$. The discrete domains become faceted as they are stabilized at very high volume fractions. Note that the curve for $n = 5$ stops at $\tau = 0.95$ due to numerical difficulties.

To investigate the effects of n on block extraction, the lamellar domain spacing D^* vs τ for $n = 3$, 4, 5, and 8 is shown in Figure 9. For $\tau < 0.4$, increasing n facilitates the extraction of the A-block from the interface as evidenced by the onset of a rapid D^* increase upon increasing τ. Steric hindrance at the s_1 junction increases with n. Thus, the onset of extraction that relieves steric hindrance at s_1 requires less bidispersity; i.e., extraction of the shorter A-block occurs closer to $\tau \approx 0.5$ as n increases. At high bidispersity, $\tau \approx 0.9$, the precipitous increase in D^* moves toward higher τ as n is increased. At high τ the miktoarm architecture suppresses extraction; extraction of the A′-segments into the B-rich domain would favor transitions toward mesophases with decreased interfacial curvature toward the A-rich domain. However, the steric hindrance about the s_1 junction strongly favors curved interfaces toward the A-rich domain, thus suppressing A′-block extraction. At $n = 8$ the A′-block extraction has become a discrete transition.

The changes in extraction with n have consequences for the location (τ) and magnitude (f_A) of the maximum deflections in phase boundaries. The bidispersity between the A- and A′-blocks relieves stretching in the A-rich domain and shifts phase boundaries toward larger f_A. Once the A- or A′-blocks are extracted from the interface, then phase boundaries shift back toward lower f_A. Thus, onset of extraction occurring closer to $\tau = 0.5$ will produce smaller deflections in phase boundaries in f_A. Likewise, an onset of extraction occurring further from $\tau = 0.5$ will produce larger deflections in phase boundaries toward larger f_A. The role of n on the phase behavior of the miktoarm $A(BA')_n$ architecture is illustrated in Figure 10a, which compares the technologically relevant S to C phase boundary at $n = 2$, 3, and 5. At low $\tau \leq 0.5$, the maximum shift in the phase boundary between the S and C phases shifts toward higher τ and lower f_A with increasing n, consistent with an onset of A-block extraction occurring closer to $\tau = 0.5$. At high values of bidispersity, i.e., $\tau \approx 0.9$, the maximum deflection moves with increasing n toward higher τ and larger f_A, again consistent with the onset of extraction occurring at higher τ.

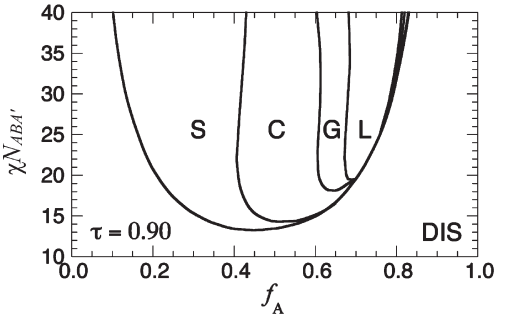

Figure 11. Phase diagram for $A(BA')_3$ at fixed $\tau = 0.9$ corresponding approximately to the largest deflection in phase boundaries toward larger f_A in Figure 7.

Although evidence of A- and A′-block extraction was shown for the lamellar morphology in Figure 9, we show contour plots of the s_2 junction density between the B- and A′-block within the C unit cell just below ($\tau = 0.85$) and above ($\tau = 0.95$) the maximal deflection in phase boundaries in Figure 10b. At $f_A = 0.5$ and $\tau = 0.85$ the s_2 junctions (white is highest density) are located at the AB-interface. As τ is increased past the maximum deflection to $\tau = 0.95$, the s_2 junction (white) has been extracted into the center of the B-rich domain.

We have carried out preliminary calculations to determine the relative fraction of B-blocks that form bridging or looping configurations between adjacent A-rich domains in the vicinity of the maximum deflection in phase boundaries near $\tau = 0.9$ for $n = 3$.[6,31] In the L morphology at $\tau = 0.85$ and $f_A = 0.7$, just before the onset of A′-block extraction from the AB-interface, the relative fraction of B-blocks forming bridging configurations is 40.1%. This value is consistent with the accepted value of bridging configurations for linear symmetric triblock copolymers in the lamellar mesophase (40−45%).[6] Increasing τ to 0.95, past the onset of A′-block extraction, the relative fraction of bridging B-blocks decreases to 28.3% due to the extraction of the smaller A′-blocks from the A-rich domains. In the C morphology at $f_A = 0.5$ and $\tau = 0.85$, a bridging fraction of 50.4% results. This value is lower than the bridging fraction in linear symmetric triblock copolymers in the C morphology (60−65%). Similar to the L morphology, the fraction of B-blocks in bridging configurations decreases once the smaller A′-blocks become dislodged from the A-rich cylinders. At $\tau = 0.95$ and $f_A = 0.5$ the bridging fraction decreases to 34.7%. Distributions of the s_2 junction with the s_1 junction fixed to a single Wigner−Seitz cell, which were used to calculate bridging fractions, are shown for L and C in Supporting Information, Figures 4 and 5, respectively.

A consequence of the stability of discrete A-rich domains at high f_A is the emergence of faceted structures resembling those in high internal phase emulsions, but on a 10 nm scale. Figure 10c shows the real space rendering of two equilibrium unit cells at $\tau = 0.9$ for the $A(BA')_5$ miktoarm architecture: S at $f_A = 0.465$ and C at $f_A = 0.66$. At $n = 5$ and $\tau = 0.9$ the S phase has been stabilized to $f_A = 0.48$, which is more than double the A-monomer loading possible with the linear ABA′. Both the S and C phases are now highly faceted in order to efficiently fill space. Periodic, faceted morphologies have previously been reported by Sioula et al. in the experimental study of miktoarm star terpolymers of styrene, isoprene, and methyl methacrylate and computationally by Grason and Kamien for a two-color (A−B) block copolymer system.[23,36] Similar faceted morphologies were observed

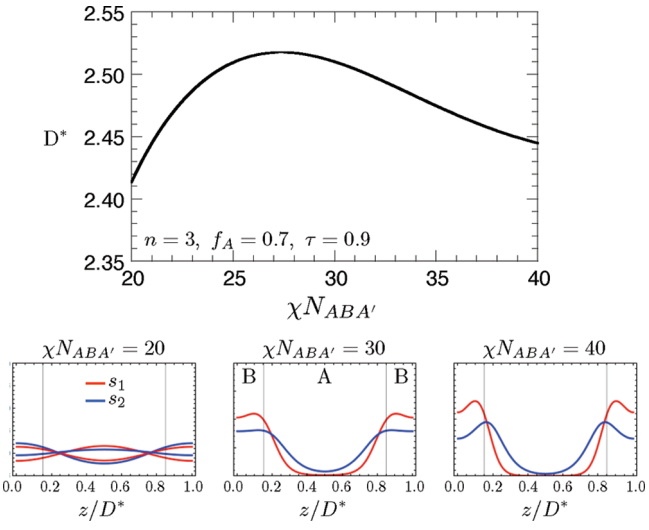

Figure 12. Lamellar domain spacing D^* vs $\chi N_{ABA'}$ with $n = 3$, $f_A = 0.7$, and $\tau = 0.9$. Junction distributions at three segregation strengths are shown below ($\chi N_{ABA'} = 20$, 30, and 40) with the location of the AB-interfaces indicated by vertical lines. At $\chi N_{ABA'} = 20$, the mesophase is weakly segregated and the junctions are mixed nearly uniformly throughout the system. As $\chi N_{ABA'}$ is increased to 30, D^* increases as the degree of segregation increases and the s_1 and s_2 junctions become excluded from the A-rich domain. The s_1 junction is more closely localized at the AB-interface than the s_2 junction, which is mixed uniformly in the B-rich domain. As χN is increased further, the s_1 and s_2 junctions localize at the interface. D^* is given in units of the unperturbed radius of gyration.

computationally for linear ABCA tetrablock copolymers by Drolet and Fredrickson.[31]

Figure 11 shows the phase diagram for the $A(BA')_3$ architecture as a function of $\chi N_{ABA'}$ and f_A at a bidispersity ratio ($\tau = 0.9$) corresponding closely to the maximum deflection in phase boundaries in Figure 7. The phase diagram is highly asymmetric with disproportionately large regions in the phase diagram occupied by S and C phases of discrete A-rich domains. The boundary between the S and C phases shifts toward lower f_A as the segregation strength is decreased, although this trend reverses close to the order−disorder boundary. We expect that thermal fluctuations not accounted for in SCFT will modify the topology of the phase diagram close to the ODT and break the critical point near $f_A = 0.7$ and $\chi N_{ABA'} = 19$. Thus, the very weakly ordered region of the phase diagram should be viewed with some skepticism. Investigation of the junction distributions within the C mesophase at $f_A = 0.5$ as a function of $\chi N_{ABA'}$ (see Supporting Information Figure 3) reveals the cause of the shift in the S to C phase boundary at intermediate segregation. As χN is increased, the s_2 junctions migrate from the B-rich domain to the AB-interface. This relaxes the A-rich domain as the bidisperse A- and A′-blocks are brought into the same microphase-separated domain. The S to C phase boundary is thus shifted toward larger f_A as $\chi N_{ABA'}$ increases.

We next examine the lamellar domain spacing as a function of $\chi N_{ABA'}$ at $f_A = 0.7$, $\tau = 0.9$, and $n = 3$ shown in Figure 12 along with junction density distributions at $\chi N_{ABA'} = 20$, 30, and 40. At low $\chi N_{ABA'} \approx 20$ the structure is weakly microphase-separated. The lamellar domain spacing D^* increases as $\chi N_{ABA'}$ is increased until $\chi N_{ABA'} \approx 27$ where D^* reaches a maximum and begins to decrease as $\chi N_{ABA'}$ is further increased. The decrease in D^* is due to the A′-blocks localizing at the AB-interface from the B-rich domain as $\chi N_{ABA'}$ is increased; this increases stretching in the B-rich domain and causes the modest decrease in D^*. These changes in the lamellar structure as $\chi N_{ABA'}$ is increased are consistent with the changes in junction density distributions with the C unit cell at $f_A = 0.5$ (Supporting Information Figure 3).

Conclusions

We have designed two potential architectures for thermoplastic elastomers (TPEs) *in silico* that would stabilize discrete A-rich domains to high f_A. The architectures we explored as TPEs were radial $(ABA')_n$ and miktoarm $A(BA')_n$ star-block copolymers. Self-consistent-field theory calculations predict that these architectures stabilize the spherical and cylindrical phases at higher volume fractions of the A-blocks than in conventional thermoplastic elastomers based on linear ABA′-triblock copolymer melts. The phase behavior in both architectures is governed by a competition between relaxing elastic stress in the A-rich domains at modest end-block bidispersity (τ), which shifts phase boundaries toward larger f_A, and the extraction of the short A′-block into the B-rich domain at high τ, which shifts phase boundaries back toward smaller f_A. A balance of both effects leads to a maximum deflection in the S−C and C−G phase boundaries at a high τ (between 0.8 and 0.9) that represents the optimum set of morphological conditions for TPEs, i.e., conditions where the A spheres or cylinders remain discrete at high f_A, thereby preserving a soft continuous B-rich domain for low modulus and good elastic recovery, but offering the promise for improved strength. We emphasize that our new designs provide these 2-fold shifts in the value of f_A at the S−C and C−G phase boundaries at modest segregation strengths without sacrificing the accessibility of the order−disorder transition. This facilitates ease of processing at temperatures above T_{ODT}.

Increasing the number of arms in the radial $(ABA')_n$ architecture had no sizable effect on the extraction of the shorter A-end blocks and therefore was of limited benefit in providing further shifts in phase boundaries. In contrast, increasing n in the miktoarm $A(BA')_n$ copolymer drove the onset of extraction to higher τ, thus allowing further shifts in phase boundaries toward larger f_A. Remarkably, in the case of five arms and $\tau = 0.9$, the body-centered-cubic S morphology was found to be stable to $f_A = 0.48$ and the hexagonal C phase was stable to $f_A = 0.7$, at which point the discrete S and C domains develop facets. Such mesophase morphologies are without precedent in conventional binary AB or ABA block copolymer systems.

In summary, we have identified novel block copolymer designs that should provide excellent combinations of properties that are desirable in TPE applications: high melt processability, low modulus, good elastic recovery, and high strength. These designs can be realized in broad classes of materials with glassy A-blocks and rubbery B-blocks. In the specific case of styrenic block copolymers prepared by anionic polymerization, the $(ABA')_n$ and $A(BA')_n$ designs should be manufacturable at commercial scale.

Acknowledgment. The authors thank Kraton Polymers LLC for financial support. F.T.O. thanks Prof. Eric Cochran and Dr. Dominik Duchs for helpful discussions regarding the numerical implementation of the SCFT equations and the AFRL DSRC for computer resources. This work was partially supported by the NSF REU Site Program through Award NSF-DMR06-49312. This work made use of MRL central facilities and was partially supported by the MRSEC Program of the National Science Foundation and under Award DMR05-20415.

Supporting Information Available: Metastable phase boundary between hexagonally packed cylinders (C) and the lamellae (L) for the $(ABA')_n$ architecture (Figure 1); lamellar domain spacing D^* vs τ for both the $(ABA')_n$ and $A(BA')_n$

architectures (Figure 2); contour plots of the chain-end/junction distributions for the $A(BA')_3$ architecture in the hexagonal morphology (Figure 3); bridging/looping configurations in the lamellar morphology (Figure 4); bridging/looping configurations in the cylindrical morphology (Figure 5). This material is available free of charge via the Internet at http://pubs.acs.org.

References and Notes

(1) Holden, G. *Understanding Thermoplastic Elastomers*; Hanser Publishers: Munich, 2000.
(2) Holden, G.; Kricheldorf, H. R.; Quirk, R. *Thermoplastic Elastomers*; Hanser Publishers: Munich, 2004.
(3) Weidisch, R.; Gido, S. P.; Uhrig, D.; Iatrou, H.; Mays, J.; Hadjichristidis, N. *Macromolecules* **2001**, *34*, 6333.
(4) Sperling, L. H. *Introduction to Physical Polymer Science*; John Wiley and Sons: New York, 2001.
(5) Helfand, E.; Wasserman, Z. R. *Macromolecules* **1976**, *9*, 879.
(6) Matsen, M. W.; Thompson, R. B. *J. Chem. Phys.* **1999**, *111*, 7139.
(7) Leibler, L. *Macromolecules* **1980**, *13*, 1602.
(8) Bates, F. S.; Fredrickson, G. H. *Phys. Today* **1999**, *52*, 32.
(9) Bates, F. S.; Fredrickson, G. H. *Annu. Rev. Phys. Chem.* **1990**, *41*, 525–557.
(10) Matsen, M. W. *J. Phys.: Condens. Matter* **2002**, *14*, R21.
(11) Sides, S. W.; Fredrickson, G. H. *J. Chem. Phys.* **2004**, *121*, 4974.
(12) Lynd, N. A.; Hillmyer, M. A. *Macromolecules* **2005**, *38*, 8803.
(13) Ruzette, A.-V.; Tence-Girault, S.; Leibler, L.; Chauvin, F.; Bertin, D.; Guerret, O.; Gerard, P. *Macromolecules* **2006**, *39*, 5804.
(14) Lynd, N. A.; Meuler, A. J.; Hillmyer, M. A. *Prog. Polym. Sci.* **2008**, *33*, 875.
(15) Matsushita, Y.; Noro, A.; Iinuma, M.; Suzuki, J.; Ohtani, H.; Takano, A. *Macromolecules* **2003**, 8074.
(16) Noro, A.; Iinuma, M.; Suzuki, J.; Takano, A.; Matsushita, Y. *Macromolecules* **2004**, 3804.
(17) Noro, A.; Cho, D.; Takano, A.; Matsushita, Y. *Macromolecules* **2005**, 4371.
(18) Matsen, M. W. *J. Chem. Phys.* **2000**, *113*, 5539.
(19) Ryu, C. Y.; Ruokolainen, J.; Fredrickson, G. H.; Kramer, E. J.; Hahn, S. F. *Macromolecules* **2002**, *35*, 2157.
(20) Hadjichristidis, N.; Iatrou, H.; Behal, S. K.; Chludzinski, J. J.; Disko, M. M.; Garner, R. T.; Liang, K. S.; Lohse, D. J.; Milner, S. T. *Macromolecules* **1993**, *26*, 5812.
(21) Milner, S. T. *Macromolecules* **1994**, *27*, 2333.
(22) Yang, L.; Hong, S.; Gido, S. P.; Velis, G.; Hadjichristidis, N. *Macromolecules* **2001**, *34*, 9069.
(23) Grason, G. M.; Kamien, R. D. *Macromolecules* **2004**, *37*, 7371.
(24) Mayes, A. M.; de la Cruz, M. O. *J. Chem. Phys.* **1989**, *91*, 7228.
(25) Matsen, M. W.; Schick, M. *Phys. Rev. Lett.* **1994**, *72*, 2660.
(26) Helfand, E.; Tagami, Y. *J. Chem. Phys.* **1972**, *56*, 3592.
(27) Fredrickson, G. H. *The Equilibrium Theory of Inhomogeneous Polymers*; Oxford University Press: Oxford, 2006.
(28) Fredrickson, G. H.; Ganesan, V.; Drolet, F. *Macromolecules* **2002**, *35*, 16.
(29) Ceniceros, H. D.; Fredrickson, G. H. *Multiscale Model. Simul.* **2004**, *2*, 452.
(30) Matsen, M. W.; Schick, M. *Macromolecules* **1994**, *27*, 6761.
(31) Drolet, F.; Fredrickson, G. H. *Phys. Rev. Lett.* **1999**, *83*, 4317.
(32) Tyler, C. A.; Morse, D. C. *Macromolecules* **2003**, *36*, 3764.
(33) Grason, G. M.; DiDonna, B. A.; Kamien, R. D. *Phys. Rev. Lett.* **2003**, *91*, 058304.
(34) Milner, S. T.; Witten, T. A.; Cates, M. E. *Macromolecules* **1989**, *22*, 853.
(35) Bi, L. K.; Fetters, L. J. *Macromolecules* **1976**, *9*, 732.
(36) Sioula, S.; Hadjichristidis, N.; Thomas, E. L. *Macromolecules* **1998**, *31*, 5272.